GSA Data Repository Item 2009076

Ediacaran Intracontinental Channel Flow

Tom Raimondo[1*], Alan S. Collins[1], Martin Hand[1], Althea Walker-Hallam[1,2], R. Hugh Smithies[3], Paul M. Evins[3], Heather M. Howard[3]

[1]Continental Evolution Research Group, School of Earth and Environmental Sciences, University of Adelaide, Adelaide, SA 5005, Australia

[2]Current address: Heathgate Resources, Level 4, 25 Grenfell St., Adelaide, SA 5000, Australia

[3]Geological Survey of Western Australia, Mineral House, 100 Plain St., East Perth, WA 6004, Australia

*E-mail: thomas.raimondo@adelaide.edu.au

GEOCHRONOLOGY

1. Sample preparation, operating procedures and data reduction

Titanite extraction was undertaken at the University of Adelaide by a combination of standard crushing, sieving, panning and heavy liquid techniques. Approximately 150 representative titanite grains were hand-picked from each sample and mounted in epoxy resin. All grains were then sectioned to approximately half their diameter and imaged using a Philips XL20 SEM at Adelaide Microscopy, University of Adelaide. None of the titanites showed any form of internal zonation when viewed under BSE. Additional photography was performed in transmitted and reflected light at Curtin University, Perth, to identify grain inclusions, morphology and topography (Fig. DR2). The mount was then evaporatively coated with about 500 nm of high purity gold.

U-Th-Pb analysis of titanite was conducted using SHRIMP II at the John de Laeter Centre for Mass Spectrometry at Curtin University, Perth. Detailed operating procedures for SHRIMP II are outlined by Williams (1998), while operating techniques specific to titanite are described by Kinny (1997). U-Pb fractionation was corrected using the Khan standard (Kinny, 1997; Kinny et al., 1994), and data reduction was completed using KRILL software (Kinny, 1997).

Due to the very low radiogenic compositions of the titanites (Table DR2), corrections for initial lead are a major consideration. Appreciable fractions of common Pb were detected for all samples, with *f* 204 values (i.e., the fraction of common ^{206}Pb in total ^{206}Pb, based on measured ^{204}Pb/^{206}Pb) ranging from 0.03–0.78 (Table DR3). Common Pb corrections were thus applied to all titanite analyses using KRILL software (Kinny, 1997), with contemporaneous common Pb compositions determined following the method of Stacey and Kramers (1975). However, disproportionately high background counts were measured throughout the analytical session. This produces the strong possibility that the proportion of very low abundance isotopes (particularly ^{204}Pb) was incorrectly measured, leading to an inappropriate common Pb correction. A strong correlation between *f* 204 and ^{206}Pb/^{238}U corrected ages for all samples suggests that this was indeed the case. The Pb data were thus treated as a simple two-component mixture of radiogenic and common leads, and the true end-member compositions determined via linear regression through the uncorrected data (Frost et al., 2000; Kinny, 1997; Williams, 1998). A limitation of this approach is that it assumes concordant data, i.e., that no analytical point has been affected by radiogenic Pb loss subsequent to geological closure. The validity of this assumption can only be assessed from the robustness of the data-defined regression, the amount of extrapolation required, and the realism of the calculated intercepts.

In order to estimate the initial Pb composition of each sample, Yorkfit regressions were applied to the uncorrected $^{238}U/^{206}Pb$ vs. $^{207}Pb/^{206}Pb$ isotope ratios (along with their associated errors) using Isoplot/Ex 3.00 (Ludwig, 2003). This method fits a least-squares regression through the data with individual data point errors taken into account (a 'Model 1' fit). The mean square of weighted deviates (MSWD) of the regression is acceptable for all samples, ranging from 1.15 to 2.15. In addition, the calculated $^{207}Pb/^{206}Pb$ intercepts (0.814–0.928) closely correspond to the Stacey-Kramers bulk Earth $^{207}Pb/^{206}Pb$ ratios applicable to Ediacaran times (0.874 at 560 Ma; Stacey and Kramers, 1975). This implies a strong likelihood that the data-defined regression represents a true two-component mixture between a single common Pb end-member (estimated from the $^{207}Pb/^{206}Pb$ intercept) and a geologically meaningful radiogenic composition. The latter is determined from the lower concordia intercept of the $^{238}U/^{206}Pb$ vs. $^{207}Pb/^{206}Pb$ array when plotted on a Tera-Wasserburg concordia diagram (Tera and Wasserburg, 1972). For each sample, the Tera-Wasserburg regression was anchored to a common Pb composition estimated from the respective Yorkfit intercept. High positive weighted residuals (>2.5) were not recorded for any sample, reinforcing the suggestion that they had not suffered Pb loss. However, a small number of analyses contained high negative weighted residuals, and were removed on the basis that they have probably been affected by inherited Pb.

2. Metamorphic reactions controlling titanite growth

Unbroken and euhedral titanite grains are commonly aligned parallel to needles of biotite and hornblende which define the mylonitic foliation. This suggests that titanite formed in equilibrium with high temperature phases during shearing. Iron oxide tails and abundant opaque inclusions indicate that its Ti content is largely sourced from ilmenite replacement. It is also commonly in contact with plagioclase grains featuring clinozoisite rims, suggesting that Ca is sourced from the breakdown of anorthite. This is consistent with the uniformly sodic composition of metamorphic plagioclase in all samples, compared to the more calcic composition of igneous grains. Furthermore, garnet rims feature an increase in grossular content, and usually contain clinozoisite inclusions. This indicates that garnet production came at the expense of clinozoisite during prograde metamorphism. Titanite growth can thus be inferred from the following reaction:

$$\text{Ca-Pl} + \text{Czo} + \text{Ilm} + \text{Qtz} \rightarrow \text{Na-Pl} + \text{Ttn} + \text{Grt} \qquad (1)$$

This process involves the modification of prograde mineral assemblages, suggesting that titanite formation occurred at peak metamorphic conditions.

3. Interpretation of age estimates

If the closure temperature for titanite is below the peak conditions attained during metamorphism, then age estimates have the potential to reflect the cessation of Pb diffusion, rather than the timing of initial titanite growth. Frost et al. (2000) estimate a closure temperature of ~660 °C for grains with a diffusive radius of 100 μm and a cooling rate of 10 °C/Ma, while Cherniak & Watson (2001) calculate a temperature of ~600 °C using the same parameters. Given that thermobarometry from the Bates region indicates temperatures in excess of 750 °C, it is quite plausible that their corresponding age estimates could coincide with cooling below Pb closure, rather than initial growth at peak metamorphic conditions.

The validity of the above inference depends crucially on two relationships. Firstly, diffusion radius increases with increasing grain size, allowing large grains to have higher closure temperatures relative to small grains (Cherniak and Watson, 2001; Frost et al., 2000). This raises the possibility that large grains may be impervious to Pb diffusion at temperatures approaching their crystallization conditions, reducing the likelihood of age resetting. Secondly, effective diffusive volume decreases with increasing grain size. This is because diffusion operates most efficiently at grain boundaries. Pb transfer will thus be confined to the periphery of large grains, preserving significant internal volumes unaffected by diffusion. In contrast, Pb exchange in smaller grains will be much more extensive, allowing a volumetrically greater proportion to undergo re-equilibration. This has two important implications: (1) the core domains of large grains will be disconnected from diffusion pathways, preventing disruption to their initial U-Th-Pb systematics; (2) the core domains of small grains may be in direct communication with grain boundaries, making them vulnerable to Pb diffusion and resetting. In other words, age estimates from larger grains are more likely to coincide with crystallization events, while those from smaller grains will usually reflect cooling below Pb closure.

Titanites from samples 187323 and 187337 are significantly larger (*c.* 500 μm ave. diameter) than those from sample 184495 (*c.* 200 μm ave.), while those from sample 155731 are intermediate between the two (*c.* 350 μm ave.). The effective diffusive radius on the largest grains (250 μm) is thus potentially 2.5 times greater than that on the smallest grains (100 μm), indicating that the former will have an appreciably elevated closure temperature relative to the latter. Furthermore, it is likely that the volumetric proportion affected by diffusion will be consistently lower for larger grains, increasing the probability of minimal disturbance to their U-Th-Pb systematics. Thus, assuming that all samples experienced similar cooling rates, and since the majority of SHRIMP analyses were positioned at grain cores, it is predicted that their estimated ages should systematically reduce with decreasing grain size. This is precisely what is observed, and allows some constraints to be placed on the events recorded by their respective age determinations. Given their large grain size, age estimates from samples 187323 and 187337 (*c.* 570 Ma) are interpreted to reflect the timing of initial titanite crystallisation. In contrast, geochronological data from samples 155731 (*c.* 550 Ma) and 184495 (*c.* 540 Ma) are interpreted to represent the progressively later timing of Pb closure as a function of decreasing grain size and increasingly extensive volumetric diffusion.

REFERENCES CITED

Cherniak, D.J., and Watson, E.B., 2001, Pb diffusion in zircon: Chemical Geology, v. 172, p. 5-24.

Close, D., Scrimgeour, I.R., and Edgoose, C.J., 2003, Compilation of geochronological data from the northwestern Musgrave Block, Northern Territory: Northern Territory Geological Survey, Technical Report, 2003-006.

Edgoose, C.J., Scrimgeour, I.R., and Close, D.F., 2004, Geology of the Musgrave Block, Northern Territory: Darwin, Northern Territory Geological Survey, Report 15, 44 pp.

Frost, R.B., Chamberlain, K.R., and Schumacher, J.C., 2000, Sphene (titanite): phase relations and use as a geochronometer: Chemical Geology, v. 172, p. 131-148.

Gregory, C., Buick, I.S., Hermann, J., and Rubatto, D., 2007, Timing of prograde upper amphibolite metamorphism and partial melting during the Petermann Orogeny, *in* Collins, A.S., Hand, M., Schmidt-Mumm, A., Buckman, S., Direen, N., Kelsey, D.E., Rutherford, L., Brick, R., and Clark, C., eds., Deformation in the Desert Conference (Geological Society of Australia, Specialist Group in Tectonics and Structural Geology): Alice Springs, Northern Territory, Abstracts, p. 42.

Kinny, P.D., 1997, Users guide to U-Th-Pb dating of titanite, perovskite, monazite and baddeleyite using the W.A. SHRIMP: Curtin University of Technology, Perth, W.A. Isotope Science Research Centre Report no. SPS 693/1997/AP72, 21pp.

Kinny, P.D., McNaughton, N.J., Fanning, C.M., and Maas, R., 1994, 518 Ma sphene (titanite) from the Khan pegmatite, Namibia, southwest Africa: A potential ion-microprobe standard, Eighth International Conference on Geochronology, Cosmochronology and Isotope Geology Abstracts: Berkeley, US Geological Survey Circular 1107, p. 171.

Ludwig, K.R., 2003, Isoplot/Ex, rev. 3.00: A Geochronological Toolkit for Microsoft Excel: Berkeley Geochronology Center Special Publication, v. 4, 71pp.

Scrimgeour, I.R., Close, D., and Edgoose, C.J., 1999, Petermann Ranges, Northern Territory (Second Edition). 1:250 000 geological map series explanatory notes, SG 52-07: Darwin, Northern Territory Geological Survey, 59 pp.

Stacey, J.S., and Kramers, J.D., 1975, Approximation of terrestrial lead isotope evolution by a two-stage model: Earth and Planetary Science Letters, v. 26, p. 207-221.

Tera, F., and Wasserburg, G.J., 1972, U-Th-Pb systematics in three Apollo-14 basalts and the problem of initial Pb in lunar rocks: Earth and Planetary Science Letters, v. 14, p. 281-304.

Williams, I.S., 1998, U-Th-Pb Geochronology by Ion Microprobe, *in* McKibben, M.A., Shanks III, W.C., and Ridley, W.I., eds., Applications of microanalytical techniques to understanding mineralising processes, Volume 7, Reviews in Economic Geology, p. 1-35.

FIGURE CAPTIONS

Figure DR1. A: S-C fabric developed in porphyritic granite from the Mt. Charles Thrust, indicating N-directed kinematics. Pen is aligned parallel to C-plane. B: Feldspar delta-clast in felsic mylonite from the northern Bates region, indicating SW-directed kinematics. Scale bar (10 cm) is aligned parallel to mylonitic foliation. Location of geochronology sample 187323. C:

Feldspar delta-clast in garnet-bearing mylonite from the western Mann Ranges, indicating WSW-directed kinematics. Finger is aligned parallel to mylonitic foliation.

Figure DR2. Transmitted light images of representative titanite grains showing the locations of SHRIMP spots (red circles). A: Sample 187337. B: Sample 187323. C: Sample 184495.

TABLE DR1. SUMMARY OF EXISTING GEOCHRONOLOGICAL DATA FROM NW MUSGRAVE BLOCK

Age (Ma)	Method	Location	Reference
561 ± 11	SHRIMP U-Pb zircon	South of Woodroffe Thrust	Scrimgeour et al., 1999
c. 555	SHRIMP U-Pb zircon and allanite	Western Mann Ranges	Gregory et al., 2007
494 ± 59	Sm-Nd mineral isochron	Eastern Mann Ranges	Scrimgeour et al., 1999
550 ± 11	Sm-Nd mineral isochron	Olia Chain	Close et al., 2003; Edgoose et al., 2004
c. 570	Rb-Sr biotite	Pottoyu Hills	Scrimgeour et al., 1999
c. 600	Rb-Sr biotite	Pottoyu Hills	Scrimgeour et al., 1999
568 ± 5	K-Ar muscovite	Petermann Ranges	Scrimgeour et al., 1999
586 ± 5	K-Ar muscovite	Petermann Ranges	Scrimgeour et al., 1999
565 ± 9	K-Ar hornblende	South of Woodroffe Thrust	Scrimgeour et al., 1999

TABLE DR2. SUMMARY OF TITANITE SIZE AND ISOTOPIC CHEMISTRY

Sample	Location*	Size range (μm)	No. grains/ No. spots	Th/U ratio range	Average U (ppm)	Average *f* 204 (%)	Age estimate (Ma)
184495	0491863 E 7140895 N	150 - 350	13/13	0.22 - 0.44	302	0.08	539 ± 4
187323	0480390 E 7157417 N	250 - 750	15/15	0.14 - 0.23	69	0.18	572 ± 7
187337	0486861 E 7149675 N	250 - 550	14/14	0.08 - 0.76	27	0.44	573 ± 14
155731	0487000 E 7146000 N	200 - 500	10/10	0.13 - 0.31	32	0.40	552 ± 12

* All coordinates derived from the Map Grid Australia Zone 52J (MGA94)

TABLE 3. SHRIMP U-Th-Pb AGE DATA

Spot name	U (ppm)	Th (ppm)	Th/U	Pb (ppm)	*f* 204 (%)	Isotope Ratios* $^{204}Pb/^{206}Pb$	±1σ	$^{207}Pb/^{206}Pb$	±1σ	$^{208}Pb/^{206}Pb$	±1σ	$^{206}Pb/^{238}U$	±1σ	$^{207}Pb/^{235}U$	±1σ	$^{208}Pb/^{232}Th$	±1σ	rho
Sample 184495																		
495-01.1	432	94	0.22	42	0.0336	0.0019	0.0001	0.0866	0.0005	0.1599	0.0010	0.0910	0.0011	1.0859	0.0146	0.0669	0.0009	0.876
495-02.1	305	101	0.33	34	0.0513	0.0029	0.0002	0.0991	0.0007	0.2915	0.0025	0.0918	0.0011	1.2543	0.0187	0.0811	0.0012	0.827
495-03.1	238	104	0.44	26	0.0588	0.0033	0.0003	0.1085	0.0011	0.2711	0.0029	0.0927	0.0012	1.3873	0.0244	0.0576	0.0010	0.763
495-04.1	165	70	0.42	20	0.0894	0.0050	0.0003	0.1351	0.0011	0.3230	0.0028	0.0955	0.0012	1.7788	0.0288	0.0727	0.0012	0.807
495-05.1	32	8	0.25	12	0.3706	0.0246	0.0011	0.4542	0.0039	1.0907	0.0100	0.1674	0.0028	10.4844	0.2049	0.7259	0.0156	0.842
495-06.1	249	57	0.23	25	0.0594	0.0033	0.0002	0.1044	0.0008	0.1886	0.0017	0.0911	0.0012	1.3118	0.0203	0.0751	0.0012	0.820
495-07.1	380	137	0.36	44	0.0501	0.0028	0.0002	0.1023	0.0006	0.3787	0.0021	0.0913	0.0011	1.2882	0.0182	0.0959	0.0013	0.858
495-08.1	396	95	0.24	40	0.0396	0.0022	0.0001	0.0892	0.0005	0.1770	0.0014	0.0926	0.0011	1.1393	0.0161	0.0685	0.0010	0.851
495-09.1	243	57	0.23	28	0.0742	0.0042	0.0002	0.1169	0.0007	0.2655	0.0018	0.0962	0.0012	1.5507	0.0221	0.1098	0.0016	0.858
495-10.1	279	79	0.28	30	0.0632	0.0035	0.0002	0.1085	0.0007	0.2402	0.0020	0.0928	0.0012	1.3889	0.0209	0.0785	0.0012	0.835
495-11.1	222	78	0.35	24	0.0663	0.0037	0.0002	0.1101	0.0008	0.2537	0.0021	0.0918	0.0012	1.3933	0.0214	0.0666	0.0010	0.818
495-12.1	374	132	0.35	37	0.0349	0.0020	0.0002	0.0884	0.0006	0.1928	0.0015	0.0896	0.0011	1.0926	0.0161	0.0489	0.0007	0.831
495-13.1	606	168	0.28	54	0.0289	0.0016	0.0001	0.0796	0.0005	0.1561	0.0013	0.0831	0.0010	0.9121	0.0128	0.0468	0.0007	0.853
Sample 187323																		
323-01.1	34	5	0.16	9	0.2630	0.0162	0.0010	0.3167	0.0033	0.7632	0.0084	0.1423	0.0024	6.2146	0.1291	0.6868	0.0162	0.807
323-02.1	112	19	0.17	14	0.1007	0.0057	0.0004	0.1293	0.0012	0.2453	0.0026	0.1044	0.0014	1.8618	0.0325	0.1523	0.0028	0.773
323-03.1	44	8	0.19	8	0.2068	0.0116	0.0009	0.2332	0.0026	0.5311	0.0065	0.1219	0.0020	3.9209	0.0822	0.3378	0.0078	0.779
323-04.1	94	14	0.15	11	0.0829	0.0047	0.0004	0.1238	0.0012	0.2218	0.0027	0.1013	0.0014	1.7286	0.0314	0.1498	0.0030	0.769
323-05.1	43	7	0.16	8	0.2367	0.0133	0.0010	0.2454	0.0029	0.5502	0.0072	0.1188	0.0020	4.0191	0.0879	0.4211	0.0104	0.773
323-06.1	42	8	0.20	9	0.2713	0.0152	0.0010	0.2668	0.0030	0.6339	0.0077	0.1285	0.0022	4.7262	0.1014	0.4047	0.0095	0.785
323-07.1	81	17	0.21	13	0.1505	0.0085	0.0006	0.1934	0.0018	0.4394	0.0045	0.1115	0.0016	2.9730	0.0547	0.2343	0.0047	0.800
323-08.1	27	4	0.17	7	0.3105	0.0194	0.0013	0.3665	0.0046	0.8789	0.0116	0.1422	0.0027	7.1875	0.1735	0.7482	0.0208	0.794
323-09.1	29	5	0.17	7	0.3180	0.0179	0.0012	0.3191	0.0038	0.7631	0.0096	0.1403	0.0026	6.1729	0.1425	0.6468	0.0171	0.796
323-10.1	69	16	0.23	10	0.1328	0.0075	0.0006	0.1744	0.0019	0.3804	0.0046	0.1066	0.0016	2.5632	0.0499	0.1755	0.0037	0.769
323-11.1	42	8	0.19	9	0.2322	0.0131	0.0009	0.2544	0.0028	0.5975	0.0070	0.1288	0.0021	4.5198	0.0944	0.3990	0.0092	0.788
323-12.1	113	21	0.18	13	0.0603	0.0034	0.0003	0.1146	0.0011	0.2117	0.0024	0.1008	0.0014	1.5926	0.0276	0.1159	0.0022	0.776
323-13.1	54	7	0.14	10	0.2142	0.0121	0.0008	0.2374	0.0024	0.6034	0.0065	0.1212	0.0019	3.9680	0.0782	0.5416	0.0120	0.791
323-14.1	105	18	0.17	12	0.0785	0.0044	0.0004	0.1190	0.0011	0.2168	0.0025	0.1004	0.0014	1.6474	0.0292	0.1294	0.0025	0.776
323-15.1	149	26	0.17	16	0.0518	0.0029	0.0003	0.1043	0.0009	0.1733	0.0019	0.0948	0.0012	1.3626	0.0226	0.0958	0.0017	0.786
Sample 187337																		
337-01.1	23	4	0.16	7	0.4271	0.0239	0.0012	0.3869	0.0039	0.8830	0.0095	0.1533	0.0026	8.1796	0.1711	0.8309	0.0201	0.820
337-02.1	60	17	0.29	10	0.1720	0.0097	0.0006	0.2080	0.0019	0.4628	0.0053	0.1133	0.0016	3.2488	0.0581	0.1813	0.0036	0.804
337-03.1	17	3	0.15	7	0.4151	0.0259	0.0014	0.4554	0.0050	1.0620	0.0124	0.1762	0.0034	11.0609	0.2587	1.2585	0.0358	0.824
337-04.1	39	4	0.11	8	0.2038	0.0127	0.0009	0.2707	0.0028	0.5666	0.0066	0.1197	0.0019	4.4693	0.0900	0.6050	0.0144	0.794
337-05.1	10	1	0.08	7	0.6028	0.0357	0.0021	0.5809	0.0076	1.3485	0.0186	0.2534	0.0063	20.2946	0.5983	4.4168	0.1942	0.842
337-06.1	89	17	0.20	13	0.1393	0.0078	0.0005	0.1835	0.0017	0.3612	0.0039	0.1125	0.0016	2.8453	0.0511	0.2076	0.0040	0.795
337-07.1	9	3	0.32	10	0.5172	0.0401	0.0019	0.6893	0.0077	1.6128	0.0189	0.3852	0.0099	36.6076	1.0759	1.9549	0.0681	0.878
337-08.1	17	4	0.22	9	0.4818	0.0326	0.0016	0.5463	0.0057	1.2878	0.0142	0.2143	0.0043	16.1418	0.3815	1.2354	0.0339	0.842
337-09.1	36	28	0.76	9	0.3487	0.0196	0.0010	0.3289	0.0032	0.8547	0.0087	0.1307	0.0021	5.9297	0.1182	0.1462	0.0030	0.811
337-11.1	12	2	0.18	7	0.5583	0.0346	0.0019	0.5747	0.0068	1.3749	0.0170	0.2431	0.0055	19.2621	0.5174	1.8156	0.0600	0.844
337-12.1	26	10	0.37	6	0.2661	0.0165	0.0011	0.3241	0.0037	0.7832	0.0096	0.1298	0.0023	5.8016	0.1291	0.2773	0.0066	0.793
337-13.1	10	1	0.13	8	0.7605	0.0426	0.0020	0.6672	0.0076	1.5702	0.0188	0.2833	0.0067	26.0626	0.7164	3.5143	0.1304	0.859
337-14.1	9	1	0.15	9	0.7816	0.0435	0.0021	0.6768	0.0078	1.6314	0.0198	0.3429	0.0087	31.9968	0.9351	3.6685	0.1426	0.870

* Displayed ratios are uncorrected for common Pb

TABLE 3 (cont.). SHRIMP U-Th-Pb AGE DATA

	U	Th	Th/U	Pb	*f* 204	Isotope Ratios*												
Spot name	(ppm)	(ppm)		(ppm)	(%)	$^{204}Pb/^{206}Pb$	±1σ	$^{207}Pb/^{206}Pb$	±1σ	$^{208}Pb/^{206}Pb$	±1σ	$^{206}Pb/^{238}U$	±1σ	$^{207}Pb/^{235}U$	±1σ	$^{208}Pb/^{232}Th$	±1σ	rho
Sample 155731																		
731-01.1	29	5	0.19	7	0.3724	0.0209	0.0017	0.3410	0.0051	0.7585	0.0131	0.1360	0.0033	6.3911	0.1907	0.5433	0.0192	0.803
731-02.1	37	6	0.162	7	0.2918	0.0164	0.0014	0.2777	0.0040	0.5976	0.0102	0.1180	0.0026	4.5179	0.1248	0.4342	0.0145	0.790
731-03.1	41	10	0.254	8	0.2564	0.0144	0.0012	0.2558	0.0033	0.5616	0.0087	0.1157	0.0022	4.0806	0.1006	0.2560	0.0072	0.785
731-04.1	53	9	0.176	10	0.2649	0.0149	0.0012	0.2728	0.0032	0.6008	0.0082	0.1118	0.0020	4.2071	0.0936	0.3808	0.0099	0.792
731-05.1	54	10	0.178	9	0.2204	0.0124	0.0009	0.2198	0.0026	0.4485	0.0066	0.1099	0.0019	3.3301	0.0736	0.2774	0.0072	0.778
731-06.1	12	2	0.182	9	0.7229	0.0405	0.0026	0.6364	0.0100	1.5081	0.0257	0.2762	0.0095	24.2344	0.9612	2.2868	0.1123	0.870
731-07.1	25	5	0.207	7	0.3968	0.0222	0.0017	0.3740	0.0056	0.8438	0.0144	0.1341	0.0033	6.9146	0.2079	0.5464	0.0193	0.809
731-08.1	20	6	0.313	10	0.6578	0.0369	0.0022	0.5585	0.0077	1.3206	0.0201	0.2018	0.0056	15.5398	0.5062	0.8504	0.0320	0.854
731-09.1	21	3	0.127	7	0.4340	0.0243	0.0019	0.4214	0.0062	0.9781	0.0162	0.1563	0.0041	9.0783	0.2869	1.2049	0.0481	0.829
731-10.1	25	4	0.166	7	0.3593	0.0201	0.0016	0.3643	0.0053	0.8026	0.0134	0.1406	0.0034	7.0647	0.2088	0.6812	0.0244	0.813

* Displayed ratios are uncorrected for common Pb

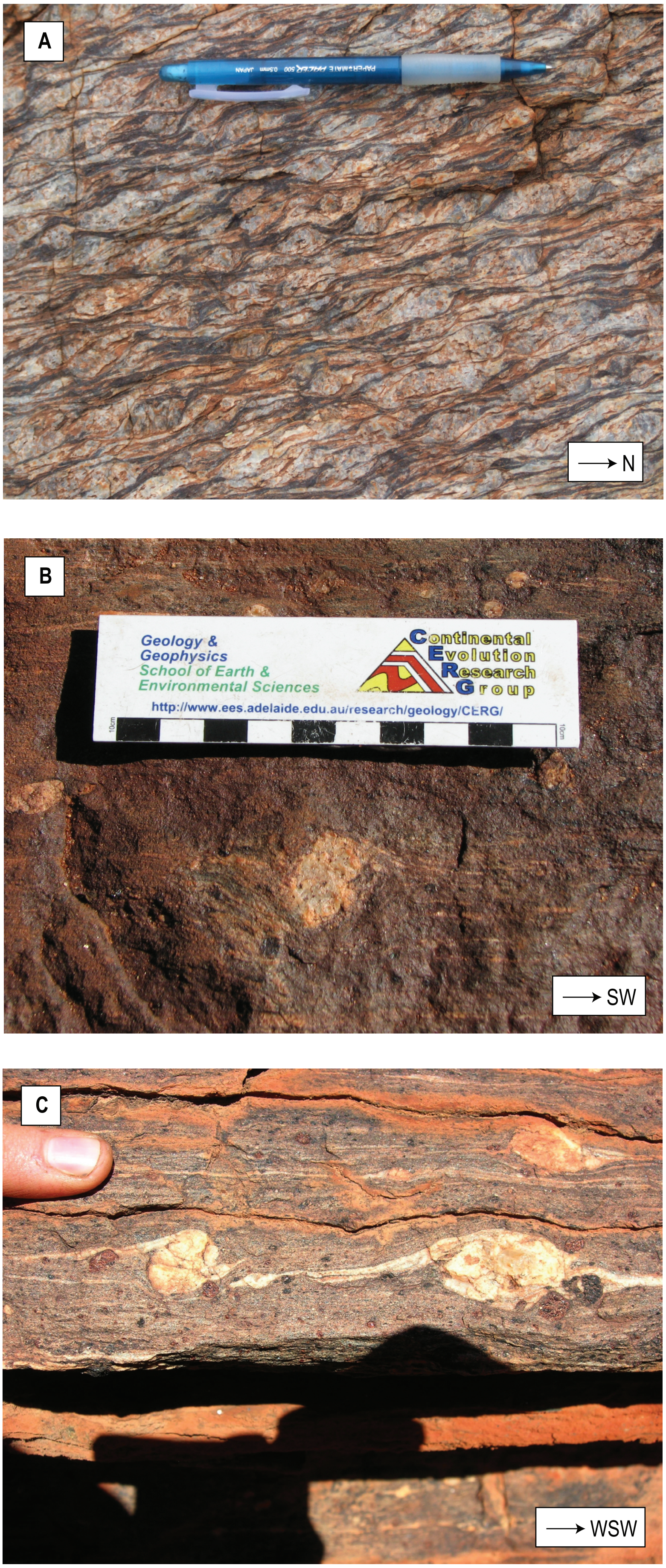

SUPPLEMENTARY FIGURE 1 - Raimondo et al. Supp Figure 1.ai

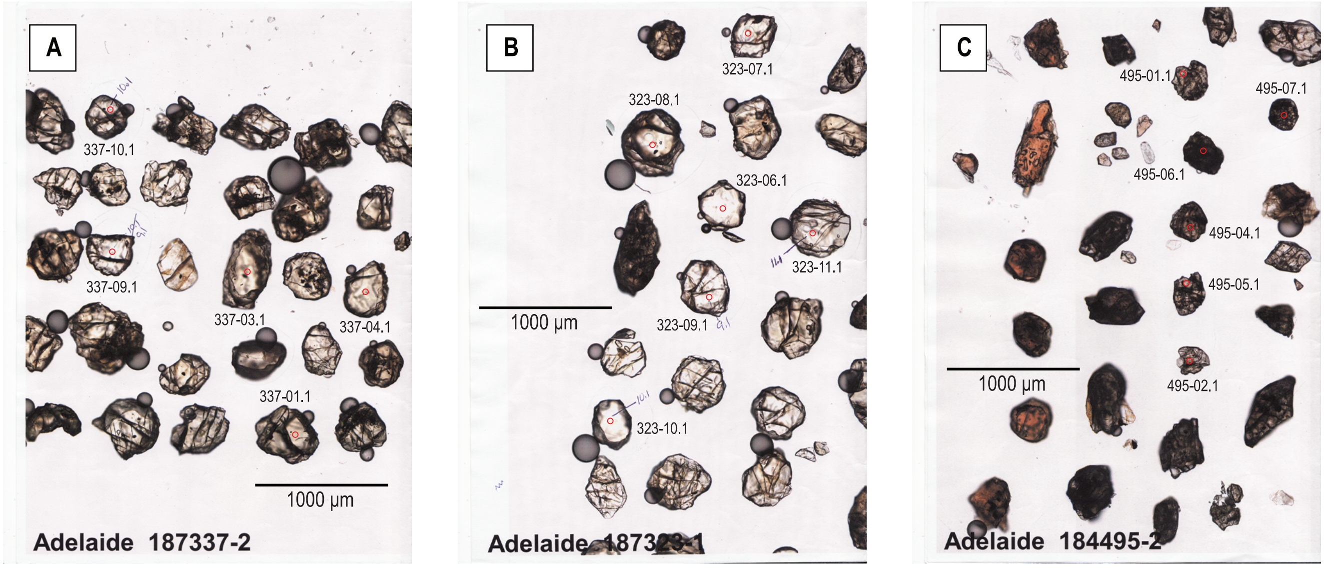

SUPPLEMENTARY FIGURE 2 - Raimondo et al.

Supp Figure 2.ai